Journal of Materials and Electronic Devices 1 (2019) 24-33

A Thermoelastic Model for Interface Strain Effects in Microscale and Nanoscale Heterostructures

Hilmi ÜNLÜ*

* İstanbul Technical University, Department of Physics Engineering Faculty of Science and Letters, Maslak 80626 İstanbul, TURKEY

We propose a thermoelastic model for strain effects in microscale planar and nanoscale cylindrical and spherical core/shell heterostructures, which takes into account the difference between lattice constants, linear thermal expansion coefficients, free thermal expansion of lattice constants and elastic stiffness constants of constituent semiconductors. Using the stress-strain relations for thermoelastic bodies, coupled with lattice mismatch induced discontinuity in elastic strain at heterointerface so called *shrink fit* condition, explicit analytical expressions are derived for interface strain in microscale heterolayers and nanoscale cylindrical and spherical core/shell heterostructure nanowires and quantum dots. Proposed model predicts that the room temperature values of in plane linear thermal expansion coefficient of GaAs thin film is identical to that of silicon substrate ($\alpha_{\parallel}(GaAs) = 2.92\times10^{-6}K^{-1}$), but smaller than in bulk GaAs ($\alpha_b(GaAs) = 5.72\times10^{-6}K^{-1}$), while the out of plane linear thermal expansion coefficient exceeds the bulk value by Poisson ratio ($\alpha_{\perp}(GaAs) = 8.57\times10^{-6}K^{-1}$), which are in excellent agreement with high resolution x-ray scattering measurements. Furthermore, lattice vibration, lattice mismatch and thermal expansion coefficients mismatch effect on core band gaps of CdSe/CdZnS and ZnSe/CdZnS QDs are calculated as a function of temperature, which are in good agreement with experimental optical absorption data. Results suggests that the proposed thermoelastic strain model can be a good predictive tool for the design of highly mismatched microscale and nanoscale heterostructure devices operating at high temperatures.

Keywords: Thermoelasticity, strain, planar heteroepitaxy, core/shell nanowires and quantum dots.

Submission Date: 23. February .2019
Acceptance Date: :10.April.2019

Corresponding author: hunlu@itu.edu.tr, Tel/Fax: +90 212 285 3201/+90 212 285 6386

1. Introduction

Advances in growing semiconductor thin films having differing physical properties with varying composition and layer thickness approaching atomic dimensions have provided new opportunities and challenges in basic scientific studies and in fabrication of electronic and optical device [1]. In addition to sophisticated growth and fabrication techniques, advancement in microscale and nanoscale semiconductor devices requires reliable and precise theoretical modelling of structural, electronic and optical properties of group IV elemental and groups III-V and II-VI binary and ternary compound heterostructures to predict their potentials. Therefore, they have received considerable attention among device scientists and engineers over almost half of a century in attempting to understand the underlying physics of interface formation and reliable modelling and precise determination of their magnitudes.

When two semiconductors with different physical properties are brought together to form a coherently strained heterostructure, difference between conduction and valence band energy levels of constituents is accommodated by discontinuities ΔE_c and ΔE_v at heterointerface,which control electronic and optical properties of constituents and charge

transport across the heterostructure. Figure 1 shows energy band diagram of Type I (a) and Type II (b) heterostructures formed between a wide bandgap semiconductor and a narrow bandgap semiconductor. In Type I heterostructures (Fig. 1a), conduction and valence bands of constituents are aligned in straddling type ($\Delta E_c = \Delta E_g - \Delta E_v$ and $\Delta E_g = \Delta E_{gB} - \Delta E_{gA}$) and in Type II heterostructures (Fig. 1b) they are aligned in staggered type ($\Delta E_c = \Delta E_g + \Delta E_v$) across heterointerface.

As the lattice constant of outer semiconductor is generally different from that of the inner semiconductor, elastic strain develops across heterointerface, which influence energy band structure of constituents. Numerous models have been proposed over the years to calculate the strain effects on electronic properties of semiconductor heterostructures [2-17]. All continuum elasticity models in case of epitaxial thin films use the original work of Frank and van der Merve [3] and Matthews and Jesser [4] and in case of core/shell nanostructures use the original work of Mott and Nabarro [5,6] and Eshelby [7]. Strain effects in two, one and zero dimensional heteroestructures have been extensively studied and is reasonably well understood at constant temperature. However, the strain effects due to linear thermal expansion coefficients difference and free thermal expansion of constituent semiconductors is still an obstacle.

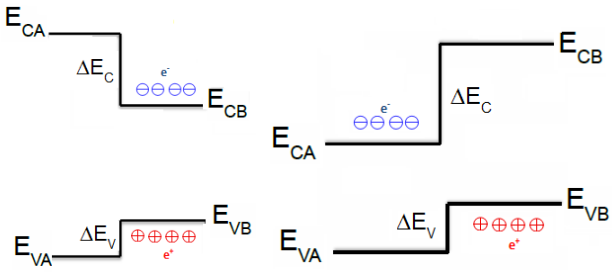

Figure 1. *Schematic band diagram of Type I (a) and of Type II (b) heterostructures.*

In this work, we will give analytical expressions for strain effects in microscale and nanostructures by using continuum elastic theory of thermoelastic bodies coupled with the discontinuity in elastic strain at heterointerface, called shrink fit condition. The paper is organized as follows: In section 2 we will give a basic review of thermoelastic strain modelling and boundary conditions in planar, cylindrical and spherical coordinates. In section 3, we give derivation of in plane and out of plane strain in heterostructures with planar geometry such as quantum wells and supelattices. In sections 4 and 5, respectively, analytical expressions will be derived for interface strain in cylindrical and spherical core/shell semiconductor heterostructures as a function of temperature. In section 6, a detailed discussion of results will be given for calculating the in plane and out of plane thermal expansion of GaAs thin film grown on Si (001) substrate and temperature dependent interface strain effects on band gap of CdSe/Cd (Zn) S and ZnSe/Cd (Zn) S core/shell quantum dots.

2. Basics of Thermoelastic Strain Model

Thermal changes in a thermoelastic body are accompanied by the shifts in relative positions of particles composing the body. Since the thermal expansion of volume elements cannot proceed freely, the total strain can be thought to consist of the sum of the thermal strain and the elastic strain produced by the resistance of the medium to thermal expansion [18,19,20]. Therefore, thermal strains are added to elastic strains due to local mechanical stress (i.e., due to lattice mismatch), so that Hooke's law is modified to the following stress-strain relations for thermoelastic bodies [18]

$$\varepsilon_{ij} = \frac{1}{E}[(1+\nu)\sigma_{ij} - \nu\sigma_{kk}\delta_{ij}] + \alpha\Delta T\delta_{ij} \quad (1)$$

where ε_{ij} and σ_{ij} are the strain and stress components, respectively. The term $\alpha\Delta$ T is the thermal strain due to temperature change . ΔT The inversion of Eq. (1) gives

$$\sigma_{ij} = \frac{E}{(1+\nu)}[\varepsilon_{ij} + \frac{\nu}{(1-2\nu)}\varepsilon_{kk}\delta_{ij}] - \frac{E}{(1-2\nu)}\alpha\Delta T\delta_{ij} \quad (2)$$

In using Eqs. (1) and (2) for strain modelling in rectangular coordinates system, the subscripts x,y, z are substituted for i and j, respectively, and cylindrical (or spherical) system of coordinates, subscripts *rr* , θθ , *zz* (or *rr* , θθ , φφ) are substituted for *i* and *j*, respectively.

In system of rectangular coordinates, the components of displacement vector in the x, y and z directions are and , respectively, and strain-displacement relations are [18]

$$\varepsilon_{xx} = \frac{\partial u_x}{\partial x}; \varepsilon_{yy} = \frac{\partial u_y}{\partial y}; \varepsilon_{zz} = \frac{\partial u_z}{\partial z} \quad (3)$$

Since we are dealing with thermoelastic body, there are no shear strains ($\varepsilon_{xy} = \varepsilon_{yz} = \varepsilon_{zx} = 0$)

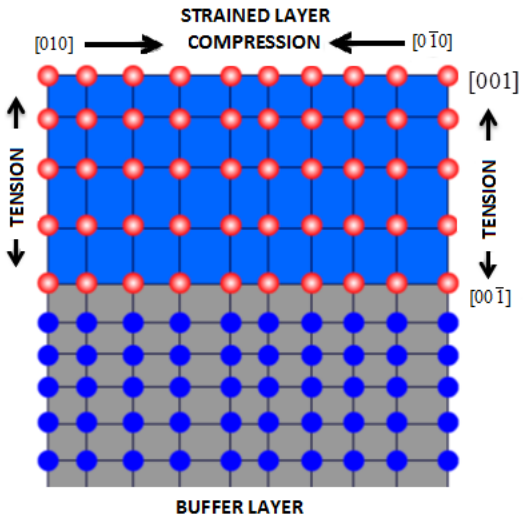

Figure 2. *Schematic view of strain effect in microscale pseudomorphic heteroepitaxy*

The use of Eqs. (1) and (2) for modelling of strain in microscale pseudomorphic heterostructures (shown in Fig. 2) are subject to the following boundary conditions: (i) stress is zero across 5 heterointerface along growth direction (out of plane), (ii) substrate is free of stress in any crystal directions, and (iii) in plane elastic strain has a lattice mismatch induced discontinuity at heterointerface, so called *shrink fit* condition, introduced here as

$$\varepsilon_{\square}^{f} - \varepsilon_{\square}^{s} = \varepsilon_m = \frac{a_s - a_f}{a_f} \qquad (4)$$

where ε_{II}^{f} and ε_{II}^{s} are in plane strains in epilayer and thick (001) substrate, respectively, and $\varepsilon_m = (a_s - a_f)/a_f$ is the lattice mismatch across epilayer/substrate heterointerface.

In system of cylindrical coordinates the components of the displacement vector in r, θ, and z directions are u_r, u_θ, and u_z and the strain-displacement relations are [18]

$$\varepsilon_{rr} = \frac{\partial u_r}{\partial r} \quad ; \quad \varepsilon_{\theta\theta} = \frac{u_r}{r} + \frac{1}{r}\frac{\partial u_\theta}{\partial \theta} \quad ; \quad \varepsilon_{zz} = \frac{\partial u_z}{\partial z} \qquad (5)$$

There are no shear strains: $\varepsilon_{r\theta} = \varepsilon_{rz} = \varepsilon_{z\theta} = 0$. In system of spherical coordinates, the displacement vector has only radial component u_r and strain-displacement relations are [18, 19]

$$\varepsilon_r = \varepsilon_{rr} = \frac{\partial u_r}{\partial r} \quad ; \quad \varepsilon_t = \varepsilon_{\theta\theta} = \varepsilon_{\varphi\varphi} = \frac{u_r}{r} \qquad (6)$$

There are no shear strains: $\varepsilon_{r\theta} = \varepsilon_{r\varphi} = \varepsilon_{\varphi\theta} = 0$ since we consider structure as thermoelastic body.

In modelling of strain effects in cylindrical and spherical core/shell heterostructures, the use of Eqs. (1) and (2) are subject to the following boundary conditions: (i) stress is continuous across the core/shell heterointerface, (i) there is no stress outside the core/shell heterostructure, and (iii) tangential elastic strain has a lattice mismatch induced discontinuity at heterointerface, so called shrink fit condition, defined as [18]:

$$[r(\varepsilon_{r\theta} - \varepsilon_{i\theta})]|_{r=a} = a\varepsilon_{im} \qquad (7)$$

Furthermore, the temperature is uniform throughout cylindrical and spherical core/shell heterostructures, which are subject to an inner and outer pressure Pi and Po, respectively (Fig. 2).

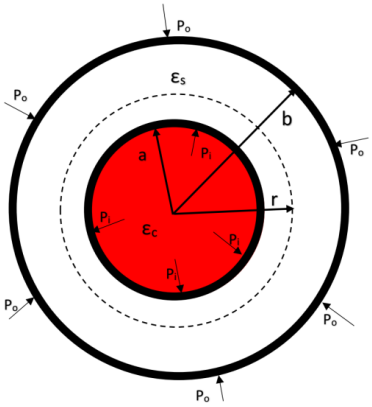

Figure 3. *Schematic cross-sectional view of core/shell cylindrical and spherical heterostructure.*

In sections 3, 4 and 5 we will use the thermoelastic stress-strain relations, definitions for strain displacements and boundary conditions given in this section to derive interface pressure and strain in microscale planar epitaxy such as quantum wells and nanoscale cylindrical and spherical core/shell heterostructures such as nanowires and quantum dots as a function of temperature.

3. Strain in Microscale Heterostructures

In modeling strain effects in microscale heterostructures (shown in Fig. 2), we can use Eq. (1) to write following relations for the in- and out- of plane strains in heterolayer on a thick substrate

$$\varepsilon_{xx}^{f} = \varepsilon_{xx}^{f} = \varepsilon_{\parallel}^{f} = \frac{a_{\parallel}^{f} - a_f}{a_f} = \frac{(1-\nu_f)}{E_f}\sigma_{\parallel}^{f} - \frac{\nu_f}{E_f}\sigma_{\perp}^{f} + \alpha_f \Delta T \qquad (8)$$

$$\varepsilon_{zz}^{f} = \varepsilon_{\perp}^{f} = \frac{a_{\perp} - a_f}{a_f} = \frac{1}{E_f}\sigma_{\perp}^{f} - \frac{2\nu_f}{E_f}\sigma_{\parallel}^{f} + \alpha_f \Delta T \qquad (9)$$

where a_{II}^{f} and $a_{\perp}^{f}$ are in- and out- of plane distorted lattice constants, and a_f is relaxed lattice constant of epilayer, respectively. $\Delta T = T - T_o = T$ is temperature change relative to $T_o = 0K$. Since stress is zero in thick substrate in all directions ($\sigma_{xx}^{s} = \sigma_{yy}^{s} = \sigma_{zz}^{s} = \sigma_{\perp}^{s} = \sigma_{II}^{s} = 0$), we can write

$$\varepsilon_{xx}^{s} = \varepsilon_{yy}^{s} = \varepsilon_{zz}^{s} = \varepsilon_{\perp}^{s} = \varepsilon_{\square}^{s} = \alpha_s T \qquad (10)$$

for strain in (001) thick substrate, where α_s is linear thermal expansion coefficient of substrate lattice constant. Equations (8), (9) and (10) are coupled with so called *shrink fit* condition, defined by Eq. (4), which describes lattice mismatch induced discontinuity in elastic strain in plane of heterostructure at interface, Substituting Eqs. (8) and (10) into Eq. (4), with continuous stress condition along growth direction ($\sigma_{\perp}^{s} = \sigma_{\perp}^{f} = 0$), one writes so called *shrink-fit* condition as

$$\frac{(1-\nu_f)}{E_f}\sigma_{\square}^{f} + \alpha_f T - \alpha_s T = \varepsilon_m \qquad (11)$$

From which one can write the in plane stress in epilayer as

$$\sigma_{\square}^{f} = \frac{E_f}{(1-\nu_f)}[\varepsilon_m + (\alpha_s - \alpha_f)T] \quad (12)$$

On substituting Eq. (12) into Eq. (8) with $\sigma_{zz}^{f} = \sigma_{\perp}^{f} = 0$ and into Eq. (9) with $\sigma_{\perp}^{s} = \sigma_{\perp}^{f} = 0$, the in plane and out of plane strain expressions, respectively, become

$$\varepsilon_{xx}^{f} = \varepsilon_{xx}^{f} = \varepsilon_{\square}^{f} = \frac{a_{\square}^{f} - a_f}{a_f} = \varepsilon_m + (\alpha_s - \alpha_f)T + \alpha_f T \quad (13)$$

$$\varepsilon_{zz}^{f} = \varepsilon_{\perp}^{f} = \frac{a_{\perp} - a_f}{a_f} = -\frac{2\nu_f}{1-\nu_f}\varepsilon_m - \frac{2\nu_f}{1-\nu_f}(\alpha_f - \alpha_s)T + \alpha_f T \quad (14)$$

Eqs. (13) and (14), respectively, reduce to $\varepsilon_{xx}^{f} = \varepsilon_{xx}^{f} = \varepsilon_{II}^{f} = \varepsilon = (a_{II}^{f} - a_f)/a_f = \alpha_f T$ for the in plane and $\varepsilon_{zz}^{f} = \varepsilon_{\perp}^{f} = (a_{\perp}^{f} - a_f)/a_f = \alpha_f T$ for out of plane distortions of lattice constant of thin film due to its free linear thermal expansion.

4. Strain in Cylindrical Core/Shell Heterostructures

We consider an infinitely long concentric cylindrical core/shell semiconductor heterostructure (cross-sectional view is shown in Fig. 3) with inner and outer radius *a* and *b* (*a*<<*b*) and is subject to an inner and outer pressure P_i and P_o. The core region is strained along z-axis due to the lattice mismatch $\varepsilon_{iz} = \varepsilon_{im} = (a_i - a_m)/a_m$ and shell region is unstrained ($\varepsilon_{zz} = \partial u_z / \partial z = 0$). Using Eq. (1) one can then write following strain-stress relations in cylindrical core/shell heterostructure as [18]

$$\varepsilon_r = \frac{a(\varepsilon_r) - a}{a} = \frac{1}{E}[\sigma_r - \nu(\sigma_\theta + \sigma_z)] + \alpha T \quad (15a)$$

$$\varepsilon_\theta = \frac{a(\varepsilon_\theta) - a}{a} = \frac{1}{E}[\sigma_\theta - \nu(\sigma_r + \sigma_z)] + \alpha T \quad (15b)$$

$$\varepsilon_z = \frac{a(\varepsilon_z) - a}{a} = \frac{1}{E}[\sigma_z - \nu(\sigma_r + \sigma_\theta)] + \alpha T \quad (15c)$$

where ε_r, ε_θ and ε_z are strain and σ_r, σ_θ and σ_z stress components, E and ν are Young's modulus and Poisson ratio, respectively.

Setting $\varepsilon_{ir} = \varepsilon_{i\theta}$ in Eqs. (15a) and (15b), one then finds $\sigma_{ir} = \sigma_{i\theta}$ and substituting this result into Eq. (15c) with $\varepsilon_{iz} = \varepsilon_{im}$ one finds following expression for stress along z-axis in core region

$$\sigma_{iz} = 2\nu_i\varepsilon_{ir} + E_i\varepsilon_{im} - E_i\alpha_i T \quad (16)$$

Substituting $\sigma_{ir} = \sigma_{i\theta} = \sigma_i = -P_i$ and σ_{iz} back into Eqs. (15a) and (15b) one finds the following expression for strain along radial and tangential direction in core region

$$\varepsilon_i = \varepsilon_{ir} = \varepsilon_{i\theta} = \frac{-(1-\nu_i-2\nu_i^2)}{E_i}P_i - \nu_i\varepsilon_{im} + (1+\nu_i)\alpha_i T \quad (17)$$

where P_i is contact pressure at core/shell interface, which is to be found from shrink fit condition.

In shell region there is no displacement along z-direction, so that strain in this direction is zero ($\varepsilon_{mz} = \partial u_{mz}/\partial z = 0$). Following Ref. 18, one writes $\sigma_{mr} = -P_i$ and $\sigma_{m\theta} = P_i$ for radial and tangential stresses inside shell region when $a \square b$ and $P_o = 0$. Stress along z-axis becomes

$$\sigma_{mz} = \nu_m(\sigma_{mr} + \sigma_{m\theta}) - E_m\alpha_m T \quad (18)$$

where E_m and ν_m are Young's modulus and Poisson ratio, and α_m is linear thermal expansion coefficient of shell, respectively. When $a \square b$ and pressure outside nanowire is zero ($P_o = 0$), Eqs. (16a) and (16b) give $\sigma_{mr} = -P_i$ and $\sigma_{m\theta} = P_i$ inside shell region. On substituting Eq. (15c) into Eqs. (15a) and (15b), ε_{mr} and $\varepsilon_{m\theta}$ then become

$$\varepsilon_{mr} = \frac{a_m(\varepsilon_{mr}) - a_m}{a_m} = -\frac{1+\nu_m}{E_m}P_i + (1+\nu_m)\alpha_m T \quad (19)$$

$$\varepsilon_{m\theta} = \frac{a_m(\varepsilon_{m\theta}) - a_m}{a_m} = \frac{1+\nu_m}{E_m}P_i + (1+\nu_m)\alpha_m T \quad (20)$$

On substituting Eqs. (17) and (20) into Eq. (7) (so called the *shrink fit* condition) one finds the internal pressure acting at cylindrical core/shell interface as

$$P_i = \frac{E_i E_m[(1-\nu_i)\varepsilon_{im} + (1+\nu_i)\alpha_i T - (1+\nu_m)\alpha_m T]}{E_m(1-\nu_i-2\nu_i^2) + E_i(1+\nu_m)} \quad (21)$$

On substituting Eq. (21) into Eq. (17) and (19) and (20), respectively, one then finds strains in core and shell regions, giving the complete solution of the strain problem in nanoscale cylindrical core/shell heterostructures when shell radius is larger than radius of core ($a \square b$).

5. Strain in Spherical Core/Shell Heterostructures

The interface strain in spherical core/shell heterostructures will be modeled by using continuum linear elastic theory of thermoelastic bodies assuming no defects or plastic deformation [18]. There is only radial displacement u_r in a hollow sphere with inner and outer radius *a* and *b* (cross-sectional wiew is shown in Fig. 3), which is subjected to a uniform temperature T and to an inner and outer pressure P_i

and P_o. Because of the spherical symmetry, stress has a radial component $\sigma_{rr} = \sigma_r$ and two tangential components $\sigma_{\theta\theta} = \sigma_{\varphi\varphi} = \sigma_t$. Using Eq. (1) strain-stress relations in spherical core and shell regions are

$$\varepsilon_r = \varepsilon_{rr} = \frac{1}{E}(\sigma_r - 2\nu\sigma_t) + \alpha T \quad (22)$$

$$\varepsilon_t = \varepsilon_{\theta\theta} = \frac{1}{E}[\sigma_t - \nu(\sigma_r + \sigma_t)] + \alpha T \quad (23)$$

Since strains and stresses are uniform in the spherical core region, we can set

$$\varepsilon_{rr} = \varepsilon_{\theta\theta} = \varepsilon_{\varphi\varphi} = \varepsilon_i \quad \text{and} \quad \sigma_{rr} = \sigma_{\theta\theta} = \sigma_{\varphi\varphi} = \sigma_i = -P_i \quad (24)$$

where ε_i and $\sigma_i = -P_i$ are, respectively, the hydrostatic interface strain and stress acting on core region. P_i is the interface contact pressure between the *i*-core and *m*-shell acting on core region. Using $\varepsilon_{rr} = \varepsilon_{\theta\theta} = \varepsilon_{\varphi\varphi} = \varepsilon_i$ and $\sigma_{rr} = \sigma_{\theta\theta} = \sigma_{\varphi\varphi} = \sigma_i = -P_i$ in Eqs. (22) and (23) one writes the following expression for strain-stress relation in core region

$$\varepsilon_i = \frac{a_i(\varepsilon_i) - a_i}{a_i} = \frac{1-2\nu_i}{E_i}\sigma_i + \alpha_i T = -\frac{1-2\nu_i}{E_i}P_i + \alpha_i T \quad (25)$$

where E_i and ν_i are the Young's modulus and Poisson's ratio and α_i is linear thermal expansion coefficient of core in bulk form.

In shell region radial and tangential stresses are $\sigma_{mr} = -P_i$ and $\sigma_{mt} = \sigma_{m\theta} = \sigma_{m\varphi} = P_i/2$ when $a \square b$ and $P_o = 0$, respectively. On substituting $\sigma_{mr} = -P_i$, $\sigma_{mt} = \sigma_{m\theta} = \sigma_{m\varphi} = P_i/2$ into Eqs. (22) and (23) one then obtains the radial and tangential strains in shell region as

$$\varepsilon_{mr} = \frac{a_m(\varepsilon_{mr}) - a_m}{a_m} = \frac{1}{E_m}(-P_i - \nu_m P_i) + \alpha_m T \quad (26)$$

$$\varepsilon_{mt} = \frac{a_m(\varepsilon_{mt}) - a_m}{a_m} = \frac{1}{E_m}[(1-\nu_m)\frac{P_i}{2} + \nu_m P_i] + \alpha_m T \quad (27)$$

where E_m and ν_m are the Young's modulus and Poissons ratio and α_m is linear thermal expansion coefficient of shell. Combining Eqs. (25) and (27) with the shrink fit condition (Eq. (7)) one finds following expression for pressure at core/shell interface

$$P_i = \frac{2E_iE_m[\varepsilon_{im} + (\alpha_i - \alpha_m)T]}{(1+\nu_m)E_i + 2(1-2\nu_i)E_m} \quad (28)$$

Substituting P_i into Eq. (25) and into Eqs. (26) and (27) one then finds expression for strain in core and shell regions respectively, giving the complete solution of the strain problem in nanoscale spherical core/shell heterostructures when shell radius is larger than radius of core ($a \square b$).

6. Results and Discussion

In this section, we will present results of calculations results for interface strain effects in two, one, and zero dimensional pseudomorphic semiconductor heterostructures. We will first discuss results of our calculations on anisotropy of thermal expansion of GaAs thin film grown on Si (001) substrate. We will then show that temperature dependent interface strain effects on core band gap of CdSe/Cd (Zn)S and ZnSe/Cd (Zn)S heterostructure core/shell quantum dots.

6.1 Anisotropy of Thermal Expansion of GaAs on Si(001)

The difference between lattice parameters of GaAs and Si is 4.1% at 300 K. X-ray diffraction measurements [19] has shown that epitaxial GaAs thin films on vicinal Si (001) substrate exhibit tetragonal distortion at 300 K. The in plane thermal expansion of GaAs thin film follows the thermal expansion of Si (001) substrate. Meanwhile, the out of plane thermal expansion of GaAs thin film exceeds bulk value. The in and out of plane lattice constants as well as the bulk GaAs lattice constant all converge at about 490 ^{0}C (average value of initial growth temperature.)

Strain effect on linear thermal expansion of GaAs heterolayer grown on Si (001) substrate are obtained by defining linear thermal expansion coefficients of epilayer parallel and perpendicular to the growth direction as $\alpha_\square(T)$ and $\alpha_\perp(T)$. According to Eqs. (13) and (14) one then writes $\varepsilon_{xx}^f = \varepsilon_{yy}^f = \varepsilon_\square^f = \alpha_\square^f T$ and $\varepsilon_{zz}^f = \varepsilon_\perp^f = \alpha_\perp^f T$, respectively, which gives

$$\alpha_\square^f(T) = (\frac{\varepsilon_m(T)}{T}) + [\alpha_s(T) - \alpha_f(T)] + \alpha_f(T) \quad (29)$$

$$\alpha_\perp^f(T) = -\frac{2\nu_f}{1-\nu_f}(\frac{\varepsilon_m(T)}{T}) - \frac{2\nu_f}{1-\nu_f}[\alpha_s(T) - \alpha_f(T)] + \alpha_f(T) \quad (30)$$

which show that in pseudomorphic planar heteroepitaxy, lattice mismatch strain also contributes to in- and out- of plane linear thermal expansion coefficients. Using Eqs. (13) and (14) one can write the following expressions for the epilayer lattice constant distorted in plane and out of plane

$$a_\square^f = a_f(1+\varepsilon_\square) = a_f(1+\alpha_\square^f T) = a_f[1 + \varepsilon_m(T) + [\alpha_s(T) - \alpha_f(T)]T + \alpha_f(T)T] \quad (31)$$

$$a_{\perp}^{f} = a_f(1+\varepsilon_{\perp}) = a_f(1+\alpha_{\perp}^{f}T) = a_f[1-\frac{2v_f}{1-v_f}[\varepsilon_m(T)+(\alpha_s(T)-\alpha_f(T))T]+\alpha_f(T)T] \quad (32)$$

Temperature dependent in- and out- of plane linear thermal expansion coefficients ($\alpha_{\parallel}(T)$ and $\alpha_{\perp}(T)$) and in-and out- of plane strain distorted lattice constants ($a_{\parallel}^{f}$ and $a_{\perp}^{f}$) of GaAs epilayer on Si (001) are calculated from Eqs. (31) and (32), respectively. Elastic stiffness parameters, $C_{11f} = 11.8$ and $C_{12f} = 5.30$ (in $10^{10} dyn/cm^2$) [20] are used in calculations. The bulk lattice constants and linear expansion coefficients for GaAs and Si fitted to following expressions [21]

$$a(T) = a_0(1+A+BT+CT^2+DT^3) \quad (33)$$

$$\alpha(T)/10^{-6}K^{-1} = \frac{1}{a}\frac{\partial a}{\partial T} = B+2CT+3DT^2 \quad (34)$$

where a_0=0.565325 (0.543108) nm is bulk lattice constant of GaAs (Si) at 300 K. Constants A, B, C, and D are empirical fitting parameters [21]: A/10^{-2} = -0.147 (-0.071), B/10^{-6} K^{-1} = 4.239 (1.887), C/10^{-9} K^{-2} = 2.916 (1.934), and D/10^{-12} K^{-3} = -0.936 (-0.4544) for bulk GaAs (Si).

Figure 4a compares the temperature variation of in- and out- of plane linear thermal expansion coefficients. Meanwhile, Fig. 4b compares the temperature variation of in- and out- of plane and lattice constant of GaAs epilayer relative to its bulk value and to that of Si (001) substrate, respectively. The in plane and out of plane lattice constants as well as the bulk GaAs lattice constant all nearly converge at about 490 ^{0}C (average value of initial growth temperature.) Out of plane linear thermal expansion coefficient ($\alpha_{\perp}^{f}(T)$) of GaAs epilayer is equivalent to that of Si (001) substrate ($\alpha_{\parallel}^{s}(T) = \alpha_s(T)$), but smaller than that of bulk GaAs ($\alpha_f(T)$) over the entire temperature range. However, out of plane thermal expansion coefficient $\alpha_{\perp}^{f}(T)$ of GaAs epilayer exceeds $\alpha_{\parallel}^{f}(T)$ by Poisson ratio. Similar observation is also true for the corresponding in- and out- of plane distortions of GaAs lattice constant (Fig. 4b) over the entire temperature range. Results shown in Fig. 4a are in excellent agreement with experimental findings of Lucas et al [19], who used high resolution x-ray scattering technique to measure the anisotropy in linear expansion coefficient of GaAs grown on Si (001) substrate.

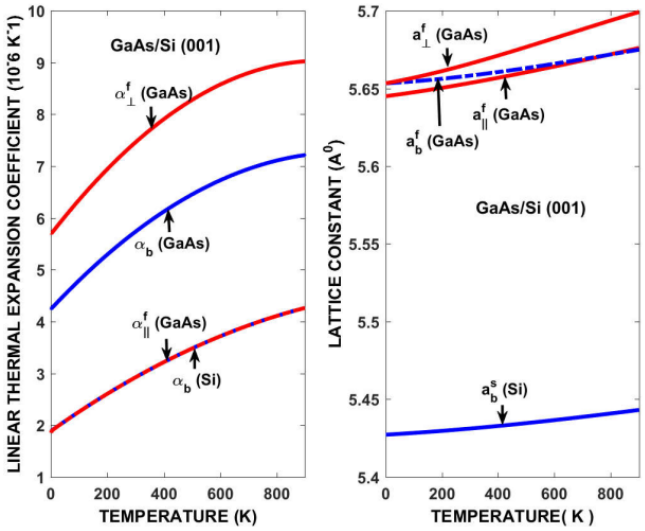

Figure 4. *Predicted temperature variation of in plane and out of plane linear thermal expansion coefficients (a) and lattice constants (b) of GaAs on Si (001).*

Table 1. compares the model calculations with experimental data of Lucas et al [19] for linear thermal expansion coefficients and lattice constants of GaAs and Si (001) at 300 K.

Table 1. Comparison of predicted and measured in plane and out of plane linear thermal expansion coefficient and lattice constant of GaAs/Si(001)

Parameter	GaAs (predicted)	GaAs (measured)	Si (Predicted)	Si (measured)
$\alpha_{\perp}(10^{-6}K^{-1})$	7.9689	8.40	3.5095	3.51
$\alpha_{\parallel}(10^{-6}K^{-1})$	3.5094	3.46	3.5095	3.46
$a_{\perp}(nm)$	0.56667	0.56602	0.5431	-
$a_{\parallel}(nm)$	0.56592	0.56483	0.5431	-

Using Eq. (12) one can determine the magnitude of in plane stress that epilayer is subject to during growth. Figure 5 shows the temperature variation of in plane stress in GaAs on Si (001) substrate. GaAs is subject to compressive in plane stress over entire temperature, but slope begins to change at around 900 K. This suggests that the proposed thermoelastic strain model could be used as part of a predictive processing

tool for planar heteroepitaxy to provide a pre-growth conditions before the actual growth process takes place.

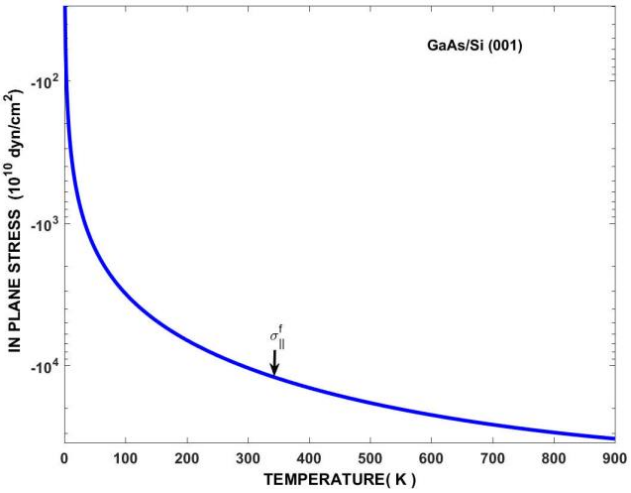

Figure 5. *Predicted temperature variation of in plane stress in GaAs on Si (001) substrate.*

6.2 Strain Effects on Core Bandgap in Core/Shell QDs

Second application of the proposed thermoelastic strain model is about predicting the interface strain shifts in band gap of type I and type II spherical heterostructure core/shell quantum dots. In a nanoscale Type I heterostructure, an electron-hole pair excited near interface tend to localize in core. Therefore, the exciton energy in core/shell nanostructures with Type-I band alignment is result of direct exciton transition inside core region. In a nanoscale Type II heterostructure, the shell conduction band edge is located in core bandgap leading to a local separation of the hole and electron in core and shell. Therefore, holes (electrons) are confined to core (shell) and electrons (holes) are confined to shell (core), which are result of indirect exciton transition. The corresponding locally indirect band gap is equal to $E_g^{id} = E_{gA} - \Delta E_c$ in hole-electron and $E_g^{id} = E_{gA} - \Delta E_v$ in electron-hole confinement, respectively.

Interface strain effects on the energy band structure of constituents of type I and type II spherical heterostructure core/shell quantum dots can be easily determined by using the so called the statistical thermodynamic model of semiconductors [22], in which one expresses the conduction and valence band edges as a function of pressure at any temperature as:

$$E_g(T,P) = E_g + \Delta C_P^0 T(1-\ln T) - \frac{a_g}{B}\left(P - \frac{P^2}{2B} - \frac{(1+B')}{3B^2}P^3\right) \qquad (35)$$

where E_g is the bulk band gap at 0 K and $a_g = -B(\partial E_g / \partial P)$ is the deformation potential. B_i is bulk modulus with its pressure derivative $B_i' = \partial B_i / \partial P$. $\Delta C_P^0 T(1-\ln T)$ is the lattice vibration contribution with temperature increase. The third term is the sum of the internal thermal pressure (i.e., volume expansion) and external pressure (i.e., due to lattice mismatch). Using Eq. (33) one can define hydrostatic pressure acting on electronic properties of core region as

$$P_i = -B_i(\varepsilon_{irr} + \varepsilon_{i\theta\theta} + \varepsilon_{i\varphi\varphi}) = -3B_i\varepsilon_i(T) = -3B_i\alpha_i T - 3B_i \frac{2E_m(1-2\nu_i)[\varepsilon_{im} + (\alpha_m - \alpha_i)T]}{E_i(1+\nu_m) + 2E_m(1-2\nu_i)} \qquad (36)$$

ΔC_P^0 is the standard state heat capacity of reaction for formation of electron-hole pair, obtained by fitting core band gap calculated from Eq. (37) at constant external pressure (without strain ε_i due to lattice mismatch) to measured bandgap [22], usually fitted to empirical Varshni expression [23]: $E_{gi}(T) = E_{gi}(0) + A/(1+BT)$, where A and B are fitting constants for bulk semiconductor.

Substituting P_i from Eq. (36) into Eq. (35) we can incorporate interface strain into conventional isotropic two band effective mass approximation [24] to determine the band gap of spherical bare and type I heterostructure core/shell QDs, given by the following equations

$$E_g^{ni}(\varepsilon_i) = E_g^{bi} + \delta E_g^{bi}(\varepsilon_i) + \frac{2\hbar^2\pi^2}{m_{cv}^* d^2} - \frac{3.572e^2}{\varepsilon_\infty d} + \frac{0.124e^4}{\hbar^2 m_{cv}^* \varepsilon_\infty^2} \qquad (37)$$

where E_g^{bi} is bandgap in bulk form at T=0 K and $m_{cv}^* = m_e^* m_h^* / (m_e^* + m_h^*)$ is reduced effective mass of electron hole pair. m_e^* and m_h^*, are effective masses of electrons and holes and ε_∞ is optical dielectric constant of core in bulk form. The third term represents confinement energy with a $1/d^2$ dependence. The fourth term represents Coulomb interaction energy with a $1/d$ dependence. Finally, last term is the Rydberg correlation energy, which is negligible when ε_∞ is large. $\delta E_{gi}^{bc}(T,\varepsilon_i)$ is the shift in core band gap due to interface strain at any temperature and hydrostatic pressure P_i, given by the following expression

$$\delta E_{gi}^{bc}(T,\varepsilon_i) = \Delta C_{iP}^0 T(1-\ln T) - \frac{a_{gi}}{B_i}\left(P_i - \frac{P_i^2}{2B_i} - \frac{(1+B_i')}{3B^2}P_i^3\right), \qquad (38)$$

where E_g^b is bandgap of core region in bulk form at T=0K.

In spherical core/shell QDs with Type II heterointerface band alignment, strain effects on core bandgap and valence and conduction band offsets can be calculated by using isotropic two band effective mass approximation according to following expression

$$E_g^{ni}(\varepsilon_i) = E_g^{bi} + \delta E_g^{bi}(T,\varepsilon_i) - \Delta E_v(\varepsilon) + \frac{2\hbar^2\pi^2}{m_{cv}^* d^2} - \frac{3.572e^2}{\varepsilon_\infty d} + \frac{0.124e^4}{\hbar^2 m_{cv}^* \varepsilon_\infty^2} \qquad (39)$$

$$E_g^{ni}(\varepsilon_i) = E_g^{bm} + \delta E_g^{bm}(T,\varepsilon_m) - \Delta E_c(\varepsilon) + \frac{2\hbar^2\pi^2}{m_{cv}^* d^2} - \frac{3.572e^2}{\varepsilon_\infty d} + \frac{0.124e^4}{\hbar^2 m_{cv}^* \varepsilon_\infty^2} \quad (40)$$

where E_g^{bi} and E_g^{bm} are, respectively, core and shell bandgaps in bulk form at T=0K, with shifts $\delta E_g^{bi}(T,\varepsilon_i)$ and $\delta E_g^{bm}(T,\varepsilon_i)$ due to strain at any temperature. Shift in band gap shell constituent of core/shell QD due to interface strain at any temperature and hydrostatic pressure P_m is given by the following expression

$$\delta E_g^{bm}(T,\varepsilon_m) = \Delta C_{mP}^0 T(1-\ln T) - \frac{a_{gm}}{B_m}\left(P_m - \frac{P_m^{\,2}}{2B_m} - \frac{(1+B_m^{'})}{3B_m^2} P_m^{\,3}\right) \quad (41)$$

where a_{gm} is bandgap deformation potential, and B_m is bulk modulus (with its pressure derivative $B_m^{'}$) of shell semiconductor in bulk form, respectively. Finally, $P_m(T,\varepsilon) = -B(\varepsilon_{mr} + \varepsilon_{m\theta} + \varepsilon_{m\varphi})$ is hydrostatic pressure acting on shell side, given as

$$P_m = -3B_m\alpha_m T - \frac{6B_m E_i[(1-2\nu_m)a^3][\varepsilon_{im} + (\alpha_i - \alpha_m)T]}{[E_i(1+\nu_m) + 2E_m(1-2\nu_i)]b^3 + 2[(1-2\nu_m)E_i - (1-2\nu_i)E_m]a^3} \quad (42)$$

In Eqs. (39) and (40), $\Delta E_v(\varepsilon)$ and $\Delta E_c(\varepsilon)$ are strain dependent valence and conduction band offsets, respectively. Hydrostatic strain effects on valence band offsets is obtained by taking difference between strain dependent valence band widths of shell and core constituents, screened by their optical dielectric constant in bulk form, and given as [25]

$$\Delta E_v(\varepsilon) = E_{mv}(\varepsilon_m)/\varepsilon_{m\infty} - E_{iv}(\varepsilon_i)/\varepsilon_{i\infty} \quad (43)$$

where $E_{iv}(\varepsilon_i)$ and $E_{mv}(\varepsilon_m)$ are strain dependent valence band edges and $\varepsilon_{i\infty}$ and $\varepsilon_{m\infty}$ are optical dielectric constants of of core and shell constituent semiconductors, respectively. Valence band widths of bulk semiconductors are determined by using density functional theory with modified Becke–Johnson exchange potential with local density approximation (mBJLDA-DFT) model [25] and hydrostatic interface strain shift is done using Eq. (23). Likewise, hydrostatic strain effects on conduction band offset is obtained by adding (subtracting) valence band offset to band gap difference, respectively, given as

$$\Delta E_c(\varepsilon) = \Delta E_g(\varepsilon) \mp \Delta E_v(\varepsilon) \quad (44)$$

where $\Delta E_c(\varepsilon) = \Delta E_g(\varepsilon) - \Delta E_v(\varepsilon)$ and $\Delta E_c(\varepsilon) = \Delta E_g(\varepsilon) + \Delta E_v(\varepsilon)$ are conduction band offsets in *Type I* and *Type II* heterostructures, respectively, with strain dependent shell and core band gap difference $\Delta E_g(\varepsilon) = E_g^m(\varepsilon_m) - E_g^i(\varepsilon_i)$. The interface strain effects on band gap of bare CdSe and ZnSe core and heterostructure core/shell CdSe/ZnS, CdSe/CdS, ZnSe/ZnS and ZnSe/CdS quantum dots are calculated by using parameters given in Table 2 for bulk CdSe, ZnSe, CdS and ZnS [21].

Table 2. Properties of some II-VI compounds used in model calculations.

Parameter/Material	CdSe	ZnSe	CdS	ZnS
a(nm)	0.607	0.5668	0.581	0.541
E_g (eV)	1.75	2.70	2.50	3.68
C_{11} (10^{10} dyn/cm^2)	7.46	8.10	7.70	1.01
C_{12} (10^{10} dyn/cm^2)	4.61	4.88	5.39	0.64
α (10^{-6} K^{-1})	3.0	7.60	3.0	6.9
A	4.09×10^{-4}	5×10^{-4}	3.45×10^{-4}	5.48×10^{-4}
B	187	218	208	282

Figure 6 compares the contribution of the effects of interface strain and lattice vibration (electron-phonon interactions) to the total band gap shift in bare CdSe and ZnSe core QDs and total shift in the core band gaps of CdSe/CdS (CdSe/ZnS) and ZnSe/CdS (ZnSe/ZnS) core/shell QDs as a function of temperature, respectively. As shown in Fig. 6, interface strain contribution to core band gap shift is positive and decreasing magnitude, while lattice vibration contribution is negative and decreasing in magnitude, with temperature increase both CdSe and ZnSe based core/shell QDs. Strain contribution to core bandgap increase is larger (about 0.30 eV) when lattice mismatch is large (e.g., in CdSe/ZnS and ZnSe/ZnS) and small (less than 0.10 eV) when lattice mismatch is small (e.g., in CdSe/CdS and ZnSe/CdS), respectively.

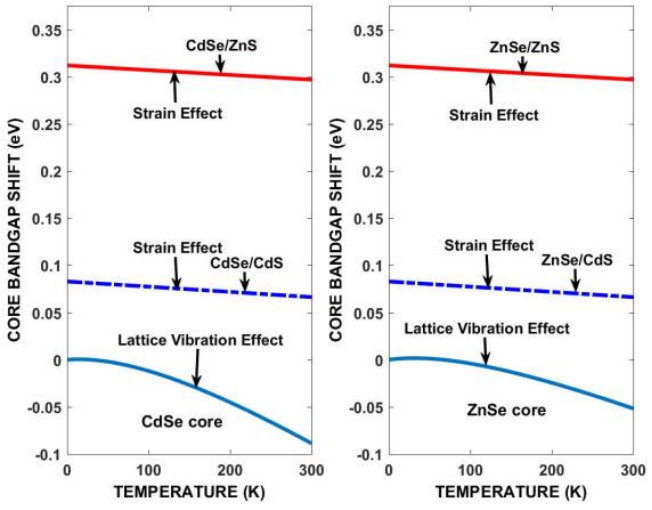

Figure 5. *The effects of interface strain and thermal vibration on band gaps of CdSe core in CdSe/CdS and CdSe/ZnS and ZnSe/ZnS and ZnSe/CdS QDs as a function of temperature.*

Figure 7 compares the effect of carrier confinement to CdSe core band gap shift in CdSe/ZnS and CdSe/CdS QDs and ZnSe core band gap shift of ZnSe/ZnS and ZnSe/CdS QDs QDs at 300 K, respectively. In both cases, carrier confinement energy contribution to shift in core bandgap is equal to combination of a $1/d^2$ and a $1/d$ dependence.

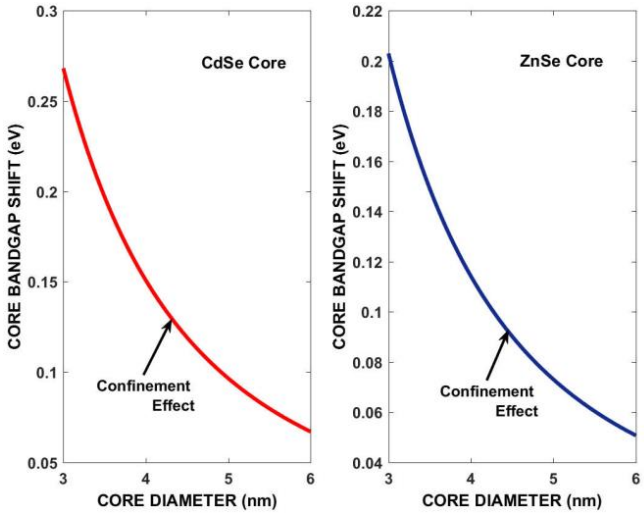

Figure 7. *The effects of carrier confinement to CdSe core band gap shift in CdSe/ZnS and CdSe/CdS QDs and ZnSe core band gap shift in ZnSe/ZnS and ZnSe/CdS QDs at 300 K.*

Combining the contributions of interface strain and lattice vibration effects to shifts in core bandgap, using the material parameters listed in Table 2, the core band gaps of bare CdSe and ZnSe core QDs and core band gaps of CdSe/ZnS, CdSe/CdS, ZnSe/ZnS and ZnSe/CdS core/shell QDs are calculated as a function of temperature. Results shown in Fig. 8 indicate that, since lattice vibration and confinement effects are same for both core and core/shell QDs, the main contribution to the increase in core band gaps of core/shell QDs is due to interface strain as a function of temperature. The results are generally in good agreement with experimental findings [26-28].

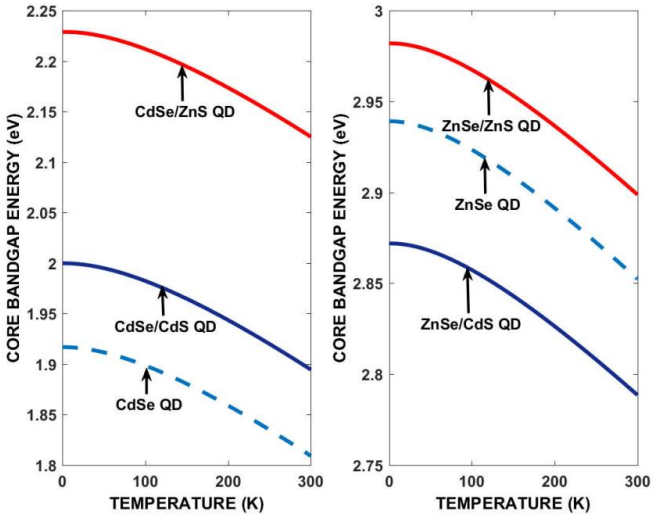

Figure 8. *Comparison of temperature variation of core band gaps of bare CdSe core QD with those of CdSe/ZnS , CdSe/CdS, ZnSe/ZnS, and ZnSe/CdS core/shell QDS.*

2. Conclusion

We discussed the effects of composition and interface strain due to lattice mismatch and thermal expansion coefficients of binary core and ternary shell on the electronic properties of constituents of CdSe/Cd(Zn)S and ZnSe/Cd(Zn)S heterostructure core/shell quantum dots as a function of temperature. It is shown that the core band gap is mainly influenced by the interface strain in heterostructure core/shell quantum dots. Consistency between theoretical predictions and experimental measurements implies that this model could be expected to be a general approach to analyze electrical and optical properties of nanoscale semiconductor systems.

Acknowledgments

The author greatly acknowledges the financial support by the Research Foundation of İstanbul Technical University (İTÜ BAP Project No: 39029).

References:

1. H. Ünlü, N. J. M. Horing and J. Dabrowski, *Low Dimensional and Nanostructured Materials and Devices*, Springer (2015).
2. G. C. Osbourne, Phys. Rev. B 27, 5126 (1983).
3. F. Frank and J. van der Merwe, Proc. R. Soc. London Ser. A **198**, 205 (1949).
4. J. Matthews and W. Jesser, Philos. Mag. **15**, 1097 (1967).
5. N. Mott and F. Nabarro, Proc. Phys. Soc. *52*, 86 **(**1940).
6. F. Nabarro, Proc. R. Soc. London Ser. A **175**, 519 (1940).
7. J. Eshelby, Proc. R. Soc. London Ser. A *241*, 376 **(**1957**).**
8. S. Suresh, A. Giannakopoulos, and M. Olsson, J. Mech. Phys. Solids **V42**, 979 (1994).

9. Balasubramanian, S., Ceder, G., & Kolenbrander, K. D. *J. Appl. Phys.* **79,** 4132-4136 (1996).
10. D. A. Faux, J. R. Downes, and E. P. O'Reilly, J. Appl. Phys. **82**, 3754 (1997).
11. A. J. Williamson and A. Zunger, Phys. Rev. B 58, 6724 (1998).
12. C. Pryor, J. Kim, L.-W. Wang, A. J. Williamson, and A. Zunger, J. Appl. Phys. **83**, 2548 (1998).
13. A. J. Williamson, A. Franceschetti, H. Fu, L. W. Wang, and A. Zunger, J. of Electronic Materials 28, 414 (1999).
14. M. Grundmann, O. Stier, and D. Bimberg, Phys. Rev. B **52**, 11969 (1995).
15. R.Maranganti and P.Sharma Handbook of Theoretical and Computational Nanotechnology (Eds. M. Rieth and W. Schommers), Volume 1, 1–44 (2005).
16. Tiberius O. Cheche, Valentin Barna, and Yia-Chung Chang, Superlattices and Microstructures 60 475 (2013).
17. D. Ferrand and Joel Cibert, Eur. Phys. J. Appl. Phys., 67, 30403 (2014).
18. A. S. Saada, Elasticity Theory and Applications (Pergamon, New York, 1974).
19. N. Lucas, H. zabel, H. Morkoç and H. Ünlü, Appl. Phys. Lett. 52, 2117 (1988).
20. O. Madelung (ed.), *Numerical Data and Functional Relationships in Science and Technology*, Vol. 17/a, Springer (1982) and Part d of Vol. 17, (1984).
21. J. E. Ayers, T. Kujofsa, P. Rago and J. Raphael, *Heteroepitaxy of Semiconductors*: Theory, Growth, and Characterization, Second Edition, CRC Press (2016).
22. H. Ünlü, Solid State Electronics, 35, 1343 (1992).
23. Y. P. Varshni, Physica, 34, 149 (1967).
24. L. E. Brus, J. Chem. Phys. 79, 5566 (1983); ibid 80, 4403 (1984).
25. H. H. Gürel and H. Ünlü, Materials Science in Semiconductor Processing, 36, 1619 (2013).
26. Abhishek Joshi, K. Y. Narsingi, and M. O. ManasrehE. A. DavisB. D. Weaver, Appl. Phys. Lett. *89*, 131907 (2006).
27. D. Valerini, A. Cretí, and M. Lomascolo, L. Manna, R. Cingolani, and M. Anni, Phys. Rev. B, *71*, 235409 **(**2005).
28. Pengtao Jing, Jinju Zheng, Micho Ikezawa, Xueyan Liu, Shaozhe Lv, Xianggui Kong, Jialong Zhao, and Yasuaki Masumoto, J. Phys. Chem. C *2009*, 113, 13545–13550.